
CHALMERS
UNIVERSITY OF TECHNOLOGY

# Experimental evaluation and theoretical prediction of single hardwood dowel connections in softwood and hardwood

Engineering Structures 353 (2026) 122251

Contents lists available at ScienceDirect

Engineering Structures

journal homepage: www.elsevier.com/locate/engstruct

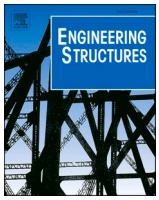

# Experimental evaluation and theoretical prediction of single hardwood dowel connections in softwood and hardwood

Inayat Ullah Khan [a,*], Mahbube Subhani [b], Kazem Ghabraie [a], Mahmud Ashraf [a]

[a] School of Engineering, Deakin University, Waurn Ponds, Geelong, VIC 3216, Australia
[b] Division of Structural Engineering, Department of Architecture and Civil Engineering, Chalmers University of Technology, Sweden

ARTICLE INFO

*Keywords:*
Wooden dowels
Double-shear connections
Joint stiffness
Maximum load capacity
Theoretical models

ABSTRACT

This study presents a comprehensive evaluation of single wooden dowel double-shear joints tested under compression loading parallel to the grain. Tasmanian Oak (a premium Australian native hardwood) was used as the dowel material, while Spotted Gum (a high-density native hardwood) and Radiata Pine (the most widely planted softwood in Australia) were used as the timber members. Wooden dowel timber-to-timber connections (WDTCs) exhibited initial elastic embedment of the dowel, followed by mixed-mode failure involving tensile bending and tensile shear. These failure modes are not accounted for in the yield limit equations of the National Design Specification (NDS) or Eurocode 5, resulting in inaccurate predictions of stiffness and load capacity for WDTCs. There is limited research on mechanics-based modelling of WDTC stiffness and capacity. In this study, several theoretical models were refined, adapted, or newly developed to predict joint stiffness, yield load, and maximum load capacity. These include beam-on-elastic-foundation models, spring-in-series models, post-test deformation–based models, embedment stiffness-based model and Johnson theory–based models for both uniform and non-uniform stress distributions. All these models are assessed against the current WDTC test data. The capacities were also compared with the new Eurocode 5 proposed yield-limit equation for WDTCs. Complementary tests, including embedment of timber with steel and wooden dowels, isolated dowel embedment, and dowel bending, were conducted to improve understanding of WDTCs behaviour and to provide input parameters for the theoretical models. The refined and newly developed mechanics-based models can be applied either independently or in conjunction with NDS models for WDTCs design.

## 1. Introduction

Dowel-laminated timber (DLT), also known as adhesive-free engineered wood products (EWPs), comprises timber layers connected using hardwood dowels. This construction method is gaining increased attention from researchers and industry [1,2]. The Interreg North-West Europe adhesive-free timber building (AFTB) initiative [3], along with over 150 projects in North America [4], demonstrates the growing adoption of DLT across diverse applications. Historically, traditional timber structures employed hardwood dowels in carpentry joints to secure structural elements, and renewed interest in all-wood construction has emerged for the authentic restoration of cultural heritage buildings [5,6].

In DLT structures, WDTCs play a critical role as the primary load-transferring elements between laminations, governing interlayer shear behaviour, stiffness development, and overall structural performance. Compared with metal fasteners, WDTCs offer advantages such as material compatibility, improved sustainability, and reduced stress concentrations [1,7]; however, their mechanical behaviour is governed by complex interactions involving shear, bending, and compression perpendicular to the grain [8]. To better understand the mechanical behaviour of WDTCs, it is informative to consider timber-to-timber connections using metal fasteners, which are well codified and provide a fundamental reference framework for analytical modelling [9]. In mechanically fastened joints, the overall performance is controlled by the fastener response and its interaction with the surrounding timber, forming a basis for comparison with WDTC behaviour and motivating the experimental and analytical investigations presented in this study. Initial studies have shown that in ductile joints, failure typically occurs when fasteners exceed their load-bearing capacity, either through bending or timber embedment at the fastener–member interface [10]. Johansen [11] was among the first to develop a mathematical

* Corresponding author.
*E-mail address:* inayat.khan@deakin.edu.au (I.U. Khan).

https://doi.org/10.1016/j.engstruct.2026.122251
Received 22 October 2025; Received in revised form 30 December 2025; Accepted 24 January 2026
Available online 29 January 2026

model—the European Yield Model (EYM)—to describe this behaviour, which later formed the basis of Eurocode 5 (EC5) and the National Design Specification (NDS) through further work by Larsen [12].

Both EC5 [9] and NDS [13] provide equations for timber-to-timber joints with metal fasteners, assuming failure occurs via fastener bending (plastic hinges) or timber embedment. While these formulations accurately predict the capacity of metal-fastened joints, they significantly overestimate the strength of WDTCs [2,14]. Subsequent experimental studies by Schmidt and Mackay [15], Schmidt and Daniels [16], and Miller et al. [8] attributed this discrepancy to the lower stiffness and different failure mechanisms of wooden dowels.

Unlike metal fasteners, wooden dowels in WDTCs fail through complex, mixed-mode mechanisms involving shear, bending, and compression perpendicular to the grain [2,14]. Schmidt and Daniels [16] identified this as Failure Mode V, also referred to as cross-grain shear failure. Failure Mode V is the shorthand term for these mixed-mode mechanisms. Accurately predicting the capacity and stiffness of WDTCs remains challenging due to these multiple interacting failure modes and the deformation of timber under dowel contact pressure. Another factor that adds complexity to wooden dowels is the inherent variability of the material itself. In contrast, the properties of metal (steel) fasteners are relatively uniform, and due to the large difference in strength and stiffness between metal fasteners and timber, moderate variations in the mechanical properties of metal fasteners have little impact on joint behaviour. For wooden dowels, however, material variability plays a significant role and can substantially influence joint performance [2,7].

Miller et al. [8] and Miller and Schmidt [6] developed empirical equations for the shear yield capacity of WDTCs using least-squares regression. The Timber Frame Engineering Council (TFEC) [17] later integrated these equations with NDS formulations to propose a design model. However, the model's applicability is limited to specific timber density ranges. Vilguts et al. [18] found that Miller's model failed to predict the strength of CLT–wooden dowel joints and proposed new regressions based on species such as Douglas Fir, Grand Fir, Western Hemlock, and Spruce-Pine-Fir with Red Oak and Birch dowels. Still, this model lacks general applicability across broader timber species. The new draft of Eurocode 5 (FprEN 1995–1-1:2024) [19] includes models for WDTCs based on Johansen yield theory [11]. Tomasi et al. [20] evaluated the Miller model and the new Eurocode 5 proposal to predict the capacity of glulam to plywood connections with dowels made of birch, beech, and laminated densified wood. They found that the Miller model underestimated the connection capacity, whereas the new EC5 proposal significantly overestimated it. The deviations observed in CLT (Vilguts et al.) and plywood connections (Tomasi et al.) can be attributed to the fact that the Miller model was not developed for such products. The Miller model was based on specific experimental conditions, with dowel diameters ranging from 19 to 28.6 mm, a substantial number being 25.4 mm. Dowel species were predominantly white and red oak, with some paper birch, sugar maple, white ash, and black locust. The timber species used as base members included yellow poplar, Eastern white pine, Douglas fir, red oak, white oak, and longleaf pine [8]. These findings highlight that the mechanical behaviour of wooden dowels is not yet fully understood, and generalised theoretical models capable of capturing the complex failure mechanisms of WDTCs and accurately predicting their load capacity remain scarce in the literature.

Another critical parameter in WDTCs is the joint stiffness ($K$) that directly influences the connection efficiency of DLT [21]. It serves as an essential input in analytical methods such as the gamma method and the shear analogy method, both of which are used to estimate the bending stiffness of mechanically jointed beams [9,10]. Eurocode 5 provides an empirical formula for the joint stiffness of metal fasteners; however, when applied to wooden dowels, it significantly overestimates the stiffness and fails to account for dowel deformation, as reported in [2,22]. Vilguts et al. [18] proposed a regression model to estimate joint stiffness for WDTCs, but its applicability is restricted to a limited range of timber species. These limitations indicate that theoretical, mechanics-based models capable of accurately predicting the joint stiffness of WDTCs are rarely available in the literature.

Australia's forests cover approximately 134 million hectares, accounting for 17 % of the continent's land area [23]. Over 70 % of this forest area consists of native hardwood species. Despite this abundance, the Australian timber industry predominantly relies on softwood, primarily Radiata Pine, for structural applications [24]. Softwood used in construction is largely sourced from commercial plantations, which occupy only 1 million hectares, with more than 70 % planted with Radiata Pine [25]. According to the Australian Bureau of Agricultural and Resource Economics and Sciences (ABARES), the supply of softwood sawlogs is expected to fall short of projected demand by 3.4 million cubic metres by 2050 [26]. To meet this growing demand, imports of softwood sawn timber will need to double between 2020 and 2050. In contrast, Australian hardwoods are dense (approximately 1000 kg/m$^3$), highly durable, and possess superior mechanical properties compared to commonly used softwoods such as Radiata Pine [27]. However, their widespread use in engineered wood products is limited by difficulties in adhesive bonding, as discussed in [28,29]. Currently, DLT production primarily uses softwood, which offers lower mechanical performance and has been reported to fail prematurely in tension under bending loads [21,30,31]. Integrating hardwood into DLT systems addresses two key limitations. First, mechanical dowel connections eliminate adhesive bonding challenges. Second, using hardwood in high-stress zones and softwood in low-stress zones enhances bending performance. Based on this concept, the present study investigates dowel-laminated connections using Radiata Pine (softwood) and Spotted Gum (high-density hardwood), mechanically connected with Tasmanian Oak hardwood dowels. Three double-shear joint configurations are examined: softwood-only joints, hardwood-only joints, and hybrid joints with hardwood side members and softwood main members.

The preceding discussion provides an overview of existing studies on WDTCs and the empirical models currently available. Despite some research on mechanically fastened timber connections, most existing studies and design models have been developed for metal fasteners, with only a limited number of empirical models applicable to WDTCs or specific timber species. Their direct applicability to WDTCs therefore remains limited due to differences in material behaviour, joint stress characteristics, and failure mechanisms. In particular, the coupled effects of shear, bending, and compression perpendicular to the grain governing wooden dowel behaviour are not explicitly addressed in current design approaches, and the associated failure mechanisms differ significantly from those of metal fastener connections. Consequently, there is a clear need for systematic experimental investigation and analytical modelling tailored to WDTCs. The present study addresses this gap by integrating experimental testing with analytical models to capture the governing failure mechanisms of WDTCs and to improve the prediction of their load-carrying capacity and stiffness. The purpose of this study is to investigate the mechanical performance of double-shear single-dowel joints incorporating three timber combinations. This research aims to characterise the mechanical properties of wooden dowel connections used in both modern DLT systems and traditional timber structures. The specific objectives are: (a) to experimentally evaluate the mechanical behaviour of wooden dowel joints, with particular focus on load capacity and failure mechanisms; (b) to assess the predictive performance of the NDS, the existing EC5, and the new EC5 proposal for WDTCs; (c) to refine existing, and develop new, theoretical models for accurate prediction of joint stiffness ($K$), yield load ($P_y$), and maximum load capacity ($P_{max}$), incorporating the effects of bearing, shear, and bending behaviour.

## 2. Materials and methods

### 2.1. Materials

Spotted Gum (SG), a high-density native Australian hardwood with excellent natural durability, and Radiata Pine (RP), a widely cultivated softwood in Australia known for its workability, were selected as the main timber materials. Tasmanian Oak (TO), a dense Australian hardwood, was used for the dowels. The compressive strength of SG and RP parallel to the grain ($f_{c||}$) was determined experimentally in accordance with ASTM D143–23 [32], and the results are presented in Table 1. For both RP and SG, specimens measuring 50 × 50 mm in cross-section and 200 mm in length were tested under a loading rate of 0.6 mm/min. The mechanical properties of TO dowels were obtained from previous studies by the authors [7,33]. In this paper, "wooden dowel" (WD) refers to Tasmanian oak (TO) dowels, and "bearing" is used synonymously with "embedment." All dowels used in the tests had a nominal diameter ($D$) of 19 mm.

The digital image correlation (DIC) system was used in all tests of this study to measure displacements at selected locations. The setup consisted of a 5-megapixel resolution camera, LED lighting, a calibration plate, a black background, and a computer for data processing. Camera calibration was performed using the calibration plate over a series of 20 images, achieving a negligible error of 0.01 pixels. The calibration plate was also used to establish the coordinate system. Prior to testing, the DIC system was validated against known displacements from the Instron loading head and synchronized with it to ensure consistency between the two measurement systems. The camera was focused on regions of interest where deformations were to be measured. These regions of interest are described in the following section for each type of test. Post-processing of the images and extraction of deformation data were carried out using Mercury RT software. DIC was used only for displacement measurement and was not configured to capture the full strain field.

All test specimens were conditioned in a standard environment of 22 °C and 65 % relative humidity, in accordance with BS EN 408:2010 [34]. The specimens were placed in a conditioning chamber until constant mass was achieved, defined as the condition where the difference between two successive weight measurements, taken at an interval of 6 h, did not exceed 0.1 % of the specimen mass. The moisture content (MC) was determined using a moisture meter, measured immediately after testing in the vicinity of the failure zone, and the values are reported in Table 1. The same procedure was followed for the material used in other tests, as discussed in the subsequent sections. Density measurements at 12 % MC were converted to specific gravity ($G$) using the procedures outlined in ASTM D2395–17 [35]. $G_{12}$ is the specific gravity at 12 % moisture content.

The following Sections 2.2, 2.3, and 2.4 describe the bending tests of TO dowels, embedment tests of timber with steel and TO dowels, and embedment tests on isolated TO dowels, respectively. While these tests may appear less directly connected, they provide essential input parameters for the analytical models presented in Section 4 ("Analytical Models"). Section 2.5 then presents the double shear tests of WDTCs, which generate experimental results that are used to validate the predictions of these analytical models.

**Table 1**
Characteristics of materials used in experimental testing ((coefficient of variation, COV, in parentheses).

| Materials | RP | SG | TO Dowel |
|---|---|---|---|
| Number of tests ($n$) | 10 | 10 | 10 |
| Mean Density ($\rho_{12}$) | 521.53 (9.47) | 1040.11 (8.65) | 630.34 (6.43) |
| MC % | 11.45 (3.45) | 10.31 (4.37) | 11.32 (5.11) |
| $G_{12}$ | 0.466 (9.47) | 0.929 (8.65) | 0.563 (6.43) |
| $G_{oven\text{-}dry}$ | 0.490 (9.47) | 1.032 (8.65) | 0.599 (6.43) |
| $f_{c\|\|}$ | 51.65 (10.63) | 72.17 (11.81) | 61.42 (8.14) |
| $f_{c\perp}$ | - | - | 8.19 (11.55) |

### 2.2. Bending tests of TO dowels

TO dowels with a diameter of 19 mm were tested under three-point bending at a loading rate of 3 mm/min in accordance with ASTM F1575 [36]. Displacement at the midsection of the dowel (at half the span) was measured using the DIC system. Black dot markers were applied along the central length of the dowel, and virtual point gauges in Mercury RT software (DIC analysis software) were used to track their movement across a series of images, enabling measurement of the corresponding displacements. Each test was continued until the dowel failed in tension and the load dropped significantly. The total length of the dowel was 200 mm, with a centre span ($L$) of 150 mm and an overhang of 25 mm on each side of the supports. All dowels failed in tension at midspan. The test setup and the corresponding force–displacement curves are shown in Fig. 1. In the figure legend, 'BE' indicates a bending test, and 'TO' refers to Tasmanian Oak. The yield load $P_y$ is determined in accordance with ASTM F1575 [36] using the 5 % offset method. A straight line is fitted to the initial linear portion of the load–displacement curve and then translated horizontally by a displacement equal to $0.05d$, where $d$ is the dowel diameter. The load at the intersection of this offset line with the load– displacement curve is taken as $P_y$. Key properties such as the bending yield moment ($M_y$), bending yield strength ($f_{yb}$), maximum bending moment ($M_{max}$), mean flexural modulus of elasticity ($E_{d,b}$), and maximum bending strength ($f_{max}$) were determined using (1) and are presented in Table 2.

$$\begin{cases} M_{\max} = \dfrac{P_{\max} L}{4} \\ M_y = \dfrac{P_y L}{4} \\ E_{d,b} = \dfrac{PL^3}{48\delta I} \\ f_{yb} = \dfrac{6M_y}{D^3} \\ f_{\max} = \dfrac{32M_{\max}}{\pi D^3} \end{cases} \tag{1}$$

### 2.3. Embedment tests of timber with steel and TO dowels

Embedment tests were conducted on RP and SG using TO dowels to determine the composite/embedment stiffness ($K_{emb}$) and embedment modulus ($k_{em}$). The term "composite" reflects the combined effect of dowel compression and localized timber deformation observed during testing. The embedment strength ($f_e$) and modulus ($k_{em}$) were calculated using Eqs. 2 and 3.

$$f_e = \frac{F_y}{D.t} \tag{2}$$

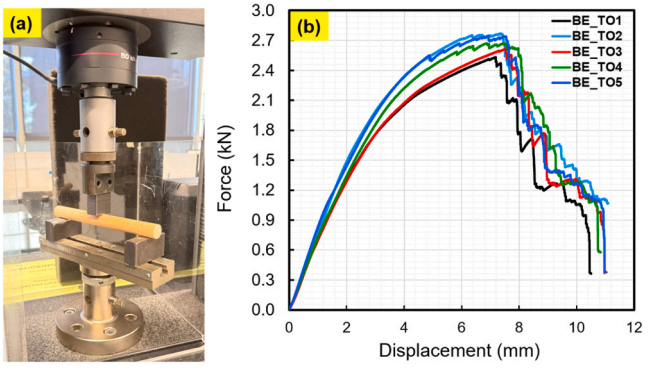


**Fig. 1.** (a) Test setup for bending tests; (b) Resulting force–displacement (P- δ) curves from the bending tests.

**Table 2**
Key results from bending tests of TO dowels (coefficient of variation, COV, in parentheses).

| Material | n | *MC* % | $P_y$ (kN) | $M_y$ (N.mm) | $f_{yb}$ (MPa) | $P_{max}$ (kN) | $M_{max}$ (N.mm) | $E_{d,b}$ (MPa) | $f_{max}$ (MPa) |
|---|---|---|---|---|---|---|---|---|---|
| Tasmanian Oak | 5 | 11.43 (5.34) | 2.41 (6.51) | 90322.5 (6.51) | 79.01 (6.51) | 2.67 (3.62) | 99987.7 (3.62) | 8809.3 (6.48) | 148.49 (3.62) |

$$k_{em} = \frac{K_{em}}{D.t} \tag{3}$$

$f_e$ represents the embedment strength determined in accordance with ASTM D5764–23a [37]. The yield load ($F_y$) was determined by fitting a linear regression to the initial elastic portion of the load–displacement curve and applying an offset of 5 % of the dowel diameter (0.95 mm for a 19 mm dowel). $f_{e,max}$ is the embedment strength determined in accordance with EN 383 [38] from $F_{max}$, defined as the maximum load reached before a displacement of 5 mm, excluding test apparatus (machine) deformation. Additional embedment tests were performed using steel dowels (SD) in both RP and SG to evaluate their embedment strength. A half-hole configuration was employed, following ASTM D5764–23a [37], to minimize dowel bending during testing. Tests were conducted under displacement control at a rate of 1.5 mm/min. For steel-dowel embedment in timber, embedment displacement was measured as the movement between the dowel centroid and the stationary base of the test machine, using a DIC virtual extensometer. For wooden dowel embedment in timber, embedment displacement was measured as the movement between the loading block and the stationary base of the test machine, using a DIC virtual extensometer. Because wooden dowels deform under load, the loading-block movement was used instead of tracking the dowel itself. The test setup for embedment of TO and steel dowels in timber is shown in Fig. 2a, and the resulting load–displacement curves are presented in Fig. 2b. In Fig. 2b, the legend identifiers RPWD and RPSD refer to the embedment of wooden dowels (WD) and steel dowels (SD) in RP, respectively. The same notation is used for SG. Specimen dimensions and key test results are provided in Table 3. For detailed information about these embedment tests, readers are encouraged to refer to the authors' article [39].

### 2.4. Embedment test on isolated TO dowel

According to BS EN 383:2007 [38], embedment strength is defined as the average compressive stress developed in a timber specimen when loaded by a rigid block. In this configuration, the fastener axis is perpendicular to the timber surface, and the applied load is perpendicular to the fastener axis, with bending not permitted. Dowel embedment testing is not specified in ASTM or EN 383; however, this reference is cited here to provide a benchmark for embedment testing. The ASTM-suggested setup (Fig. 2a) was reversed by replacing the timber block with steel and the steel dowel with a wooden dowel.

To meet the standard requirement of preventing dowel bending, the TO dowels in this study were tested using a steel loading plate, with the ends restrained by slotted-in steel angle sections and bolted connections to eliminate flexural deformation, as shown in Fig. 3a. The steel block length used for loading was 39.8 mm. Tests were conducted under displacement control at a rate of 1.5 mm/min, and displacement was measured as the movement of the 39.8 mm loading plate using the DIC system. The loading block had a semi-circular notch to replicate the embedment of the WD in timber. From the resulting load–displacement curves in Fig. 3b, the mean stiffness and embedment strength of the TO dowels were determined as 7.07 kN/mm (COV: 14.35 %) and 13.53 MPa (COV: 2.69 %), respectively. For more detailed information on these tests, readers are encouraged to refer to the authors' article [39].

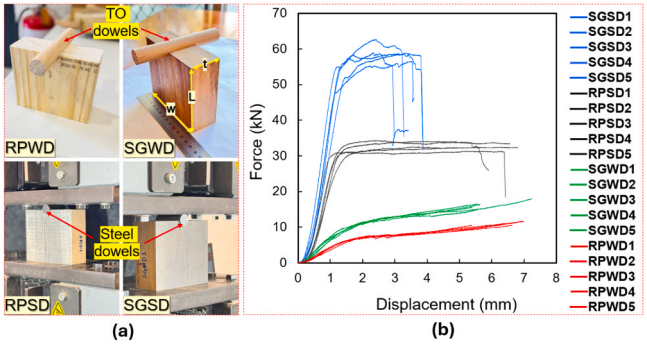


**Fig. 2.** (a) Test setup for embedment tests using steel and TO dowels in RP and SG timber; (b) Resulting force–displacement curves from the embedment tests.

### 2.5. Double shear tests of WDTCs

Double shear tests were conducted on defect-free specimens of RP and SG. Three joint configurations were evaluated: RRR, where all three members were RP; SSS, where all members were SG; and SRS, where SG was used for the side members and RP for the central member.

In all specimens, the total dowel length matched the overall thickness of the joint. Loading was applied parallel to the grain under compression. The central (main) member was extended 25 mm above the side members to allow space for vertical compression, as illustrated in Fig. 4b. Specimen preparation and loading followed the ASTM D5652–21 standard [40]. Tests were conducted using an Instron universal testing machine at a constant crosshead displacement rate of 1.5 mm/min. Slip was measured using DIC by tracking two symmetric speckle rows placed equidistant on the opposing member faces at the shear plane (Fig. 4b); the relative displacements were averaged to obtain the connection slip. Joint stiffness was determined in the linear elastic range, following ASTM D5652–21 [40] and ISO/TR 21141 [41]. End distances for both main and side members were set at four times the dowel diameter (*4D*), in accordance with ASTM D5652–21 requirements for compressive loading. Holes with a diameter of 18.95 ± 0.03 mm, slightly smaller than the 19 mm dowels, were pre-drilled, and dowels were carefully inserted by vertical hammering to ensure a tight fit. *MC* was measured both before and after testing and was approximately 11.4 %.

To prevent lateral separation of the side members during loading, steel angle sections with slotted holes were placed on each side of the joint. These sections were bolted in a way that restrained opening without applying compressive force across the joint members, as shown in Fig. 4c.

The specimen dimensions for RP were: main and side member thickness ($t_m$ and $t_s$) 45 mm, length ($L$) 175 mm, and width ($b$) 120 mm. For the SG specimens, the only difference was the thickness of the main and side members, both of which were 42 mm. The specimen dimensions were selected based on the commercially available sizes for SG (42 mm) and RP (45 mm). These sizes are also intended for use in future studies on DLT panels. The result of the double shear test is discussed in the next section.

## 3. Experimental results and discussion

### 3.1. Failure mechanism

A total of 15 single WDTCs were tested to failure under compression-induced double shear loading. As shown in Fig. 5, the WD experienced

**Table 3**
Key results from embedment tests using steel and TO dowels in RP and SG timber (coefficient of variation, COV, in parentheses).

| Materials ID | n | *MC* % | *L* mm | *w* mm | *t* mm | $f_e$ MPa | $f_{e,max}$ MPa | $K_{em}$ kN/mm | $k_{em}$ N/mm$^3$ |
|---|---|---|---|---|---|---|---|---|---|
| SGSD | 5 | 10.66 (6.32) | 100 | 120 | 42 | 72.48 (4.16) | - | 63.50 (11.06) | - |
| RPSD | 5 | 11.59 (7.23) | 100 | 120 | 45 | 37.69 (4.30) | - | 42.33 (14.71) | - |
| SGWD | 5 | 10.83 (5.43) | 100 | 120 | 42 | 14.87 (1.91) | 18.65 (4.64) | 8.82 (3.04) | 11.05 (3.04) |
| RPWD | 5 | 11.82 (5.11) | 100 | 120 | 45 | 8.75 (2.28) | 10.96 (4.46) | 6.05 (7.75) | 7.08 (7.75) |

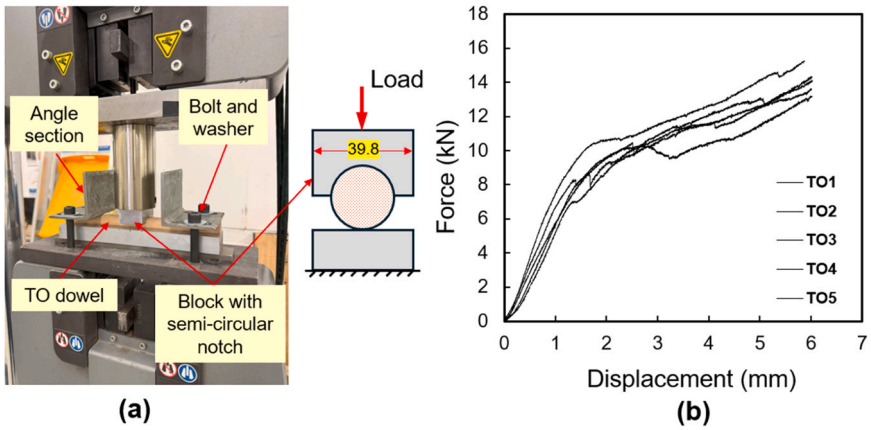


**Fig. 3.** (a) Test setup for embedment tests on isolated TO dowels; (b) Resulting force–displacement curves from the embedment tests.

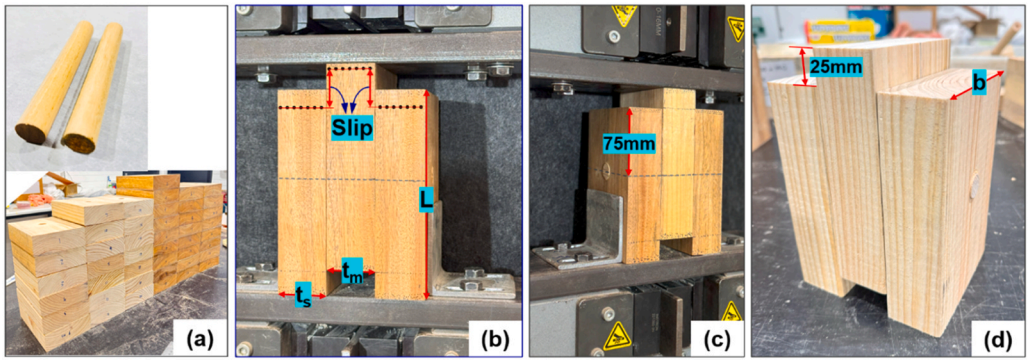


**Fig. 4.** (a) RP and SG timber with drilled holes and TO dowels (b) Double shear testing of SSS (c) SRS (d) RRR.

significant damage across all joint types, while the surrounding timber members exhibited minimal visible damage.

According to Fukuyama [42], dowels with a high slenderness ratio (λ = dowel length divided by diameter) tend to fail through shear cracking or dowel fracture. In contrast, dowels with a low slenderness ratio (λ ≤ 2) typically fail in an embedment-dominated mode. In this study, λ ranged from 6.63 to 7.11, and failure of the TO dowels was governed by combined bending and shear induced tensile stresses. Although lateral opening of the joint was restrained using bolted angle sections, minor outward tilting of the side members was still observed at higher displacements (Fig. 5c).

Fracture consistently initiated on the tension side of the dowel at crack tips located approximately 0.8–1.0 times the dowel diameter away from the shear plane on each side. Despite the brittle nature of timber, load transfer continued beyond the initial crack due to the mechanical interlocking in the fractured dowel segments, thereby preventing sudden failure. For the SSS and SRS configurations, a secondary increase in load was observed following initial yielding, with a peak occurring prior to final fracture, as shown in Fig. 6. This was also observed in 3 of the 5 RRR specimens.

No significant inward movement of the dowel or visible embedment in RP or SG members was observed. The failure mode of the TO dowels was primarily characterised by shear and bending, which differs from the yield mechanisms defined for metal fasteners in EC5, as illustrated in Fig. 5d.

### 3.2. *Force–displacement behaviour of connections*

The force–displacement response of the joints exhibited an initial linear elastic region, where the load was primarily resisted by the elastic embedment of the dowel into the timber. This linear response extended up to approximately 1.02 mm, 1.11 mm, and 1.03 mm of slip for the RRR, SRS, and SSS specimens, respectively, as shown in Fig. 6. This region was used to determine the joint stiffness. As relative slip between timber layers increased, load transfer occurred at the interface between timber members, accompanied by local dowel compression. The

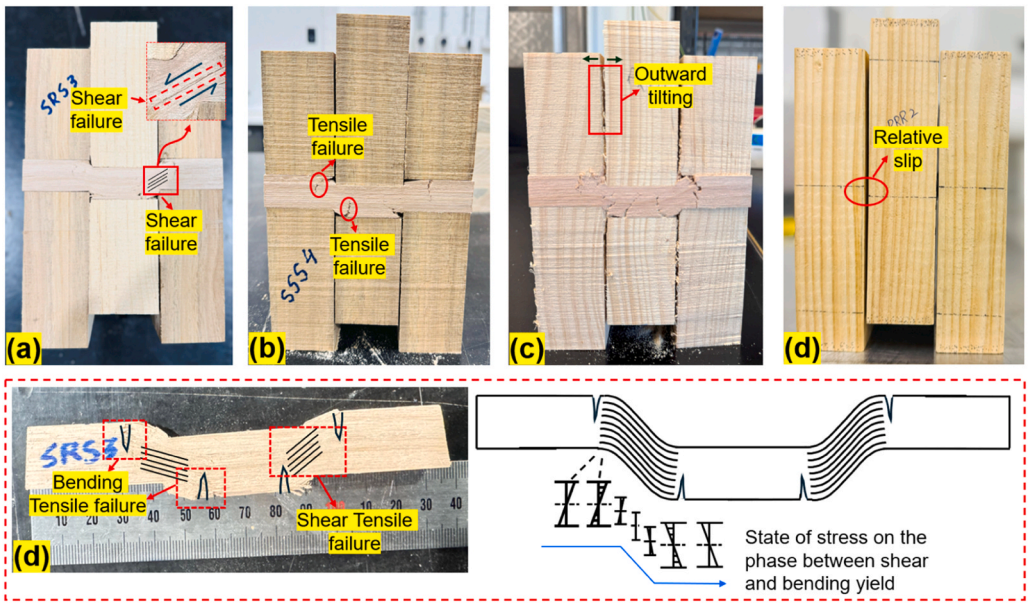


**Fig. 5.** Failures in double shear joints after testing: (a) SRS, (b) SSS, (c) RRR, (d) Dowel failure mode.

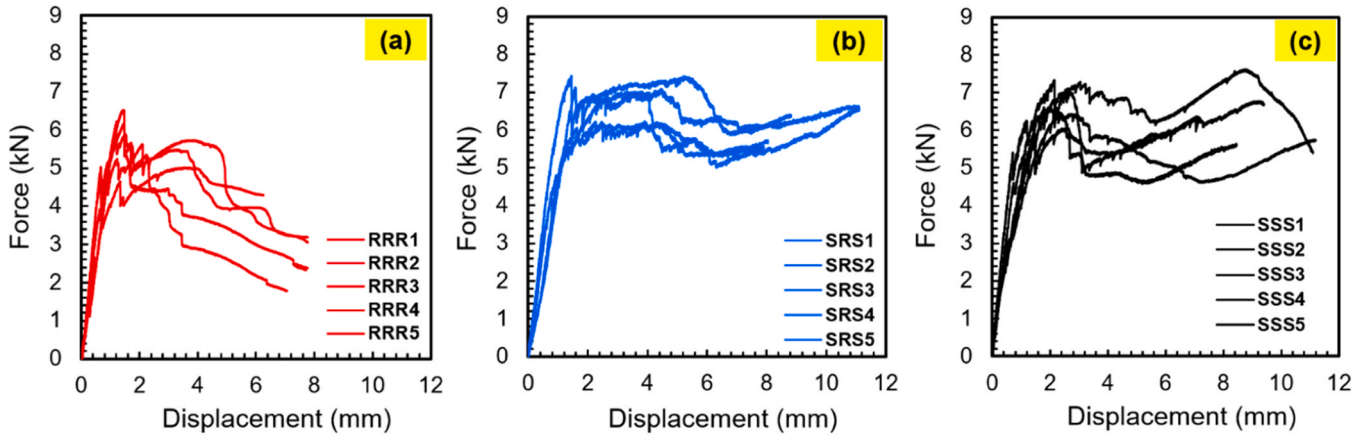


**Fig. 6.** Load displacement curves from push out tests of WDTCs: (a) RRR; (b) SRS; (c) SSS.

differential fibre movement on either side of the interface generated shear and bearing stresses in the dowel. A drop in load was observed for RRR at a mean displacement of 1.09 mm (COV 16.3 %), for SRS at 1.20 mm (COV 19.8 %), and for SSS at 1.07 mm (COV 21.1 %), likely due to shear crack formation along the grain at the timber interface, a phenomenon similarly reported in [42]. No distinct yield plateau was observed in the load–displacement curves. Therefore, the 5 % diameter offset method was used to define the yield load. In cases (RRR) where a the load is higher than the intersection point of the offset line, that value was taken as the yield load, following the procedure recommended by Schmidt and Scholl [43]. Beyond 5 mm displacement, a secondary rise in load was observed in the SSS and SRS joints, likely due to local densification of the dowel and/or tension developing after plastic hinge formation (Fig. 6). This rise begins at 6.77 mm (COV 15.43 %) for SRS and 5.04 mm (COV 21.43 %) for SSS. This effect was absent in RRR, moderate in SRS, and pronounced in SSS, indicating a progressive improvement in dowel bearing capacity from RRR to SSS. A similar secondary load increase has also been reported in previous studies [22, 44]. At approximately 10 mm displacement, the load transfer shifted from dowel bearing to the shear plane again, followed by a load drop associated with mixed bending and shear failure. Testing was terminated at this stage. Overall, the first load drop corresponds to a shear crack. This is followed by load redistribution under combined shear and tension. The third rise in load in SRS and SSS joints is likely due to densification.

The joint stiffness across the three configurations ranged from 6.05 to 7.11 kN/mm, representing a maximum variation of approximately 15 % (Table 4). The yield and maximum load capacities varied within a similar range, between 11 and 15 %. Although SG and RP have significantly different densities, the relatively small variation in mechanical performance indicates that the overall joint response is governed primarily by the dowel. This is expected, as the dowel is loaded perpendicular to the grain, while the timber members are loaded parallel to the

**Table 4**
Key Results from push-out tests of timber–to-timber connections with TO Dowels.

| Group ID | $K_{exp}$ (kN/mm) | $P_{y,exp}$ (kN) | $P_{max,exp}$ (kN) |
|---|---|---|---|
| RRR | 6.84 | 5.76 | 5.94 |
| | (5.33) | (13.63) | (9.85) |
| SRS | 6.05 | 6.52 | 6.96 |
| | (10.40) | (11.00) | (7.56) |
| SSS | 7.11 | 6.48 | 6.80 |
| | (8.79) | (7.66) | (8.92) |

grain, making dowel behaviour dominant.

During testing, the dowel initially deformed elastically through embedment, followed by failure in shear and bending at the shear plane. These results indicate that joint stiffness is largely controlled by the elastic embedment of the wooden dowel. This observation is supported by the embedment stiffness values of the TO dowel in RP (6.05 kN/mm) and SG (8.82 kN/mm), as well as in isolated bearing tests (7.07 kN/mm), presented in Table 3 and *Section 2.4*, respectively. These values closely align with the stiffnesses measured in the RRR, SSS, and SRS joints, confirming that elastic embedment of the dowel is the dominant mechanism influencing joint stiffness. This observation can be further verified using data from the literature as well as the current study, as listed in Table 5. The five values from Fu et al. [44] correspond to different side and main member thicknesses. The results indicate that in most studies the stiffness of WDTCs ranges between 0.80 and 1.00 times the embedment stiffness ($K_{em}$). Mathematically, this can be expressed as $K_{joint} = 0.80–1.00K_{em}$. The embedment stiffness of timber with a wooden dowel is slightly higher than the stiffness of WDTCs, because in WDTCs some deformation can occur at the shear planes in addition to embedment deformation, which reduces the overall stiffness. In simple terms, the factor 0.8–1 is used to account for shear and bending deformation occurring at the shear plane. This finding is significant as it may eliminate the need for additional testing of WDTCs to determine joint stiffness. By adopting $K_{joint} = 0.85K_{em}$, the ratio $K_{em}/K_{joint}$ approaches unity (Table 5). As shown in the rightmost column (highlighted in light green), the predicted values deviate by less than 20 % in most cases, with only one exception. This provides strong evidence of the reliability of this relationship, although further studies are warranted to validate and refine it.

## 4. Analytical models

The NDS and EC 5 provide yield limit equations for various failure modes ($I_m$ to $I_k$) applicable to dowel-type fasteners. An additional failure mode, designated as $I_d$, is specific to wooden dowels and was introduced by Schmidt and Daniels [16] to represent bearing failure of the dowel itself. These failure modes for single-dowel joints with double shear planes are mathematically expressed in (4) and illustrated in Fig. 7. The parameter $k_3$ is an auxiliary term introduced to simplify and shorten the expression of (4). Mode V is discussed later, as this failure mode is specific to WDTCs.

$$
\begin{cases}
P_{I_m} = f_{e,m} D t_m \\
P_{I_s} = 2 f_{e,s} D t_s \\
P_{III_s} = \dfrac{2 k_3 D t_s f_{e,m}}{(2 + R_e)} \\
P_{IV} = 2D^2 \sqrt{\dfrac{2 f_{e,m} f_{y,b}}{3(1 + R_e)}} \\
P_{I_d} = \min(D t_m f_{ed}, \quad 2 D t_s f_{ed}) \\
P_{I_j} = 2.10 \dfrac{f_{e,s} t_s D}{2 + R_e} \left[ \sqrt{2R_e(1 + R_e) + \dfrac{4R_e(2 + R_e) M_y}{f_{e,s} D t_s^2}} - R_e \right] \\
P_{I_k} = 2.30 \sqrt{\dfrac{2R_e}{1 + R_e}} \cdot \sqrt{2 M_y f_{e,s} D} \\
\text{Where } R_e = \dfrac{f_{e,m}}{f_{e,s}}, \quad k_3 = -1 + \sqrt{\dfrac{2(1 + R_e)}{R_e} + \dfrac{2 f_{y,b} (2 + R_e) D^2}{3 f_{e,m} t_s^2}}
\end{cases}
\tag{4}
$$

Failure mode $I_d$ is defined as the minimum load at which embedment occurs either in the dowel at its contact with both side members ($2t_s$) or with the main member alone. This mode can govern the joint response when the dowel has a low slenderness ratio ($\lambda \leq 2$) [42].

**Table 5**
Comparison of stiffness from experimental joint tests and embedment tests with wooden dowels.

| References | Dowel Material | Middle & side members | $K_{joint}$ | $K_{em}$ | $K_e/K_{joint}$ | $0.85K_{em}/K_{joint}$ |
|---|---|---|---|---|---|---|
| | | | kN/mm | kN/mm | - | - |
| Fu et al. [44] | Beech (Fagus) | Larch LVL | 5.43 | 6.54 | 1.20 | 1.02 |
| | | | 5.80 | 6.54 | 1.13 | 0.96 |
| | | | 5.37 | 6.54 | 1.22 | 1.04 |
| | | | 6.93 | 6.54 | 0.94 | 0.80 |
| | | | 6.57 | 6.54 | 1.00 | 0.85 |
| Zhang et al. [22] | Beech | Pinus sylvestris | 8.09 | 11.1 | 1.37 | 1.17 |
| | Beech | Spruce | 8.22 | 9.6 | 1.17 | 0.99 |
| Current study | TO | RP | 6.84 (5.33) | 6.05 (7.75) | 0.88 | 0.75 |
| | TO | SG | 7.11 (8.79) | 8.82 (3.04) | 1.24 | 1.05 |

In Fig. 7, black dots indicate the formation of plastic hinges. Mode $I_m$ represents bearing-dominated yielding of the main member in contact with the dowel, while Mode $I_s$ reflects bearing failure in the side members. Mode $III_s$ corresponds to yielding of the fastener in bending at a single plastic hinge per shear plane, combined with bearing failure in the side members. Mode *IV* involves the formation of two plastic hinges per shear plane, accompanied by localized bearing failure in both main and side members.

These theoretical models, described in (4), were applied to predict the load-carrying capacities of the RRR, SRS, and SSS joint configurations. The values $M_y = 90322$ N·mm and $f_{yb} = 79.01$ MPa were taken from Table 2, and the dowel bearing strength ($f_{ed} = 13.53$ MPa) was adopted from *Section 2.4*. Embedment strengths of the side and main timber members ($f_{e,s}$ and $f_{e,m}$) were obtained from Table 3, based on steel dowel embedment tests.

Using these input parameters, theoretical capacities were calculated and compared with experimental results in Table 6. Mode $I_d$ (wooden dowel embedment), highlighted in light green, emerges as the governing mode among the EC5 and NDS formulations, but it overestimates the connection capacity relative to the experimental results. Although Mode $I_d$ includes dowel embedment, the overprediction indicates that full embedment is not achieved in practice. None of the standard failure modes accurately predicted the load capacity of WDTCs. The results indicate that the existing yield limit models, developed for steel fasteners, do not adequately represent the failure mechanisms observed in wooden dowel joints.

For stiffness prediction, the equation provided in Eurocode 5 ((5)) for metal-based fasteners significantly overestimated the values measured in this study. These discrepancies suggest that the failure of wooden dowels is not solely governed by the European Yield Model (EYM), which considers dowel bending and timber embedment, but that dowel failure in WDTCs also includes contributions from dowel shear and compression perpendicular to the grain. This combined failure mechanism in WDTCs is referred to as Failure Mode V (Fig. 7).

$$
K_{EC5,cal} = \frac{\rho_m^{1.5} D}{23}; \textit{for SRS combination}, \quad \rho_m = \sqrt{\rho_{RP} \rho_{SG}}
\tag{5}
$$

### 4.1. New draft of EC5

Tomasi et al. [20] recently studied WDTCs and noted that the current draft of Eurocode 5, FprEN 1995–1-1:2024 [19], includes a predictive capacity model for WDTCs derived from Johansen yield theory [11]. The governing expression is given in (6). To maintain consistency with the NDS and with earlier formulations, this paper uses the notation "side member ($s$)" and "main member ($m$)" rather than EC5's "member 1" and "member 2," and writes the EC5 parameter $\beta$ as $R_e = f_{e,m}/f_{e,s}$. (6) applies

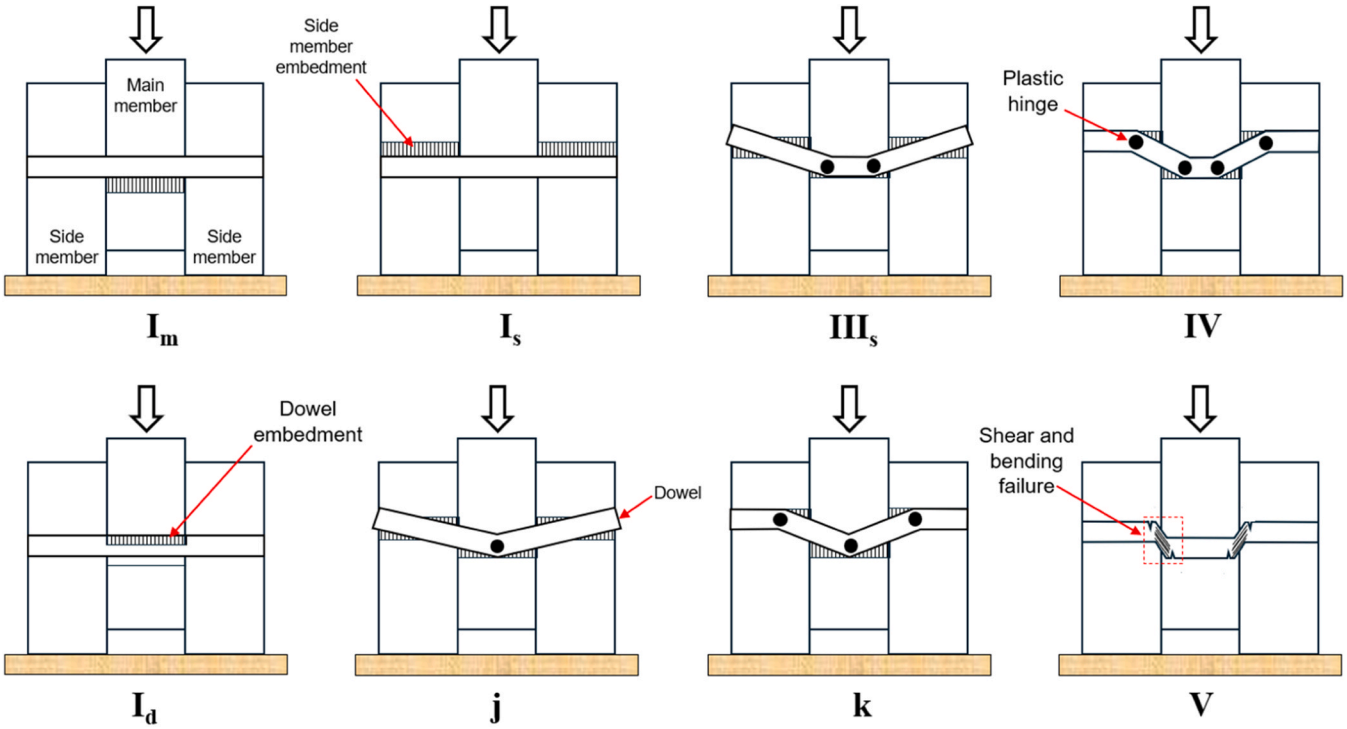


**Fig. 7.** Failure modes specific to metal dowel-connected timber–timber joints ($I_m$, $I_s$, $III_s$, IV, j, k) and wooden dowel (WD)-connected joints ($I_d$ and V).

**Table 6**
Comparison of experimental results with predictions from EC5 and NDS yield limit equations.

| Load capacity, $P_{y,\ EC5,cal}$ | | | | |
|---|---|---|---|---|
| Modes | Input values | RRR (kN) | SRS (kN) | SSS (kN) |
| $I_m$ | **Dowel:** D= 19 mm, | 32.22 | 32.22 | 57.84 |
| $I_s$ | $M_y$ = 90322 N·mm, | 64.44 | 115.68 | 115.68 |
| $III_s$ | $f_{yb}$ = 79.01 MPa, | 25.72 | 22.89 | 43.18 |
| IV | $f_{ed}$ = 13.53 MPa | 23.93 | 27.45 | 33.19 |
| $I_j$ | **RP:** t = 45 mm, $f_e$= 37.69 MPa | 27.00 | 39.54 | 45.34 |
| $I_k$ | **SG:** t = 42 mm, $f_e$= 72.48 MPa | 27.52 | 31.57 | 38.17 |
| $I_d$ | | 11.57 | 11.57 | 10.79 |
| **$P_{y,exp}$** | - | **5.76** | **6.52** | **6.48** |
| Joint stiffness, $K_{EC5,cal}$ | | | | |
| Parameter | Input values | RRR (kN) | SRS (kN) | SSS (kN) |
| $K_{EC5,cal}$ | D= 19 mm | 9.84 | 16.51 | 27.71 |
| | **RP:** 521.53 kg/m$^3$ | | | |
| | **SG:** 1040.11 kg/m$^3$ | | | |
| **$K_{exp}$** | - | **6.84** | **6.05** | **7.11** |

to connections in solid timber, plywood, cross laminated timber, laminated veneer lumber, and glued laminated timber. It is obtained by adapting Johansen's (4) as follows: (i) the coefficients 1.15 and 1.05 introduced in EC5 to account for differing partial safety factors are set to 1; and (ii) the yield moment $M_y$ is replaced by the ultimate moment $M_u$. Tomasi et al. also discussed formulations for single shear connections in the draft EC5; these are not reproduced here because the present study focuses on double shear configurations. For clarity, (6) was originally formulated with characteristic values, but here it is expressed in mean terms using the mean embedment strength, since its output is compared with the mean capacity. A factor of 2 is included to represent double shear planes.

$$\begin{cases} P_{I_m} = f_{e,m} D t_m \\ P_{I_s} = 2 f_{e,s} D t_s \\ P_{I_j} = 2\dfrac{f_{e,s} t_s D}{2+R_e}\left[\sqrt{2R_e(1+R_e)+\dfrac{4R_e(2+R_e)M_u}{f_{e,s} D t_s^2}} - R_e\right] \\ P_{I_k} = 2\sqrt{\dfrac{2R_e}{1+R_e}} \cdot \sqrt{2M_u f_{e,s} D} \end{cases} \quad (6)$$

$M_u$ can be determined from (7) in FprEN 1995–1-1:2024, where $f_m$ is the characteristic bending strength, taken as $f_{max}$. A reduction factor of 0.75 is introduced to account for the brittle behaviour of wooden dowels.

$$M_u = 0.75 \frac{\pi}{32} f_m d^3 \ for \quad 12 \le d \le 30 \quad (mm) \quad (7)$$

The draft EC5 (6) has been calibrated against embedment strengths determined in accordance with BS EN 383 [38]: therefore $f_{e,max}$ is used. For SRS joint, the lower of the SG and RP embedment strengths is used. Predictions and experimental capacities are compared in Table 7. The governing modes are highlighted in lighter green. The draft EC5 model (FprEN 1995–1-1) predicts capacities that are approximately 1.60, 1.44, and 2.04 times higher than the experimental values for RRR, SRS, and SSS connections, respectively. Consistent with these results, Tomasi et al. also reported that FprEN 1995–1-1 significantly overestimates capacity.

Current NDS and EC5 yield equations do not accurately predict either the capacity or the stiffness of WDTCs. This highlights the need for revised formulations that better capture the complex failure behaviour of wooden dowel connections. To address this gap, both existing models were critically evaluated, and new theoretical approaches were developed to more accurately predict the stiffness, yield load, and maximum load capacity of WDTCs. (4) has not been modified or improved, as it is a mechanics-based formulation derived specifically for the failure modes shown in Fig. 7. One of the main contributions of this study is the evaluation of the applicability of existing regression models and the

**Table 7**
Comparison of experimental results with predictions from the new draft of EC5.

| Load capacity, $P_{y,cal}$ | | | | |
|---|---|---|---|---|
| Modes | Input parameters | RRR (kN) | SRS (kN) | SSS (kN) |
| $I_m$ | **Dowel:** $D$= 19 mm, | 9.37 | 9.37 | 14.88 |
| $I_s$ | $M_u$ = 74992.7 N·mm, | 18.74 | 29.77 | 29.77 |
| $I_j$ | **RP:** t = 45 mm, $f_{e,max}$= 10.96 MPa | 9.23 | 11.78 | 13.22 |
| $I_k$ | **SG:** t = 42 mm, $f_{e,max}$= 18.65 MPa | 11.18 | 9.62 | 14.58 |
| $\mathbf{P_{y,exp}}$ | β= 0.588 | **5.76** | **6.52** | **6.48** |

proposal of new predictive models. The following sections focus on capacity and stiffness prediction models for failure Mode V (sketched in the bottom-right corner of Fig. 7).

### 4.2. Theoretical models for joint stiffness

#### 4.2.1. Beam on elastic foundation

Eurocode 5 provides an empirical joint stiffness equation that accounts only for the elastic deformation of the timber members. However, in WDTCs, deformation occurs in both the timber members and the dowels. Therefore, this study adopts a beam-on-elastic-foundation (BEF) approach to determine the elastic stiffness of WDTCs. Details of this method can also be found in a previous study [45].

The BEF model, which accounts for the bending as the primary deformation mechanism, is commonly used to calculate the initial stiffness of joints with metal fasteners. The governing differential equation is given in (8), where $y(x)$ represents the displacement at a distance $x$, and $EI$ is the flexural rigidity of the dowel.

$$y^{(4)}(x) + \frac{k_{em}D}{EI}y(x) = 0 \tag{8}$$

However, when the fastener is made of wood, which exhibits pronounced anisotropy (direction-dependent mechanical properties), the predictions from a beam-on-elastic-foundation (BEF) model that excludes shear deformation deviate significantly from those incorporating shear effects. To account for this, the general beam equation including shear deformation ((9)) is reformulated into (10) and further reduced to the differential form presented in (11). This formulation describes a beam resting on an elastic foundation with an embedment modulus $k_{me}$, subjected to a distributed reaction force $w(x)$ from the foundation. The resulting transverse deflection at a position $x$ along the beam is denoted by $y(x)$, as illustrated in Fig. 8a.

$$M(x) = -EI\left(\frac{k'}{GA}w(x) + y''(x)\right) \tag{9}$$

$$w(x) = -k_{em}Dy(x) = -EI\left(u_1 y''(x) - y^{(4)}(x)\right) \tag{10}$$

$$y^{(4)}(x) - u_1 y''(x) + u_2 y(x) = 0 \tag{11}$$

$$where\ u_1 = \frac{k'k_{em}D}{GA},\quad u_2 = \frac{k_{em}D}{EI}$$

Here, $EI$ and $GA$ represent the flexural and shear stiffness of the wooden dowel, respectively (i.e. $EI$=$E_{db}I_d$ and $GA$=$G_{d,}A_d$. The term $k'$ is the shear correction factor, defined as the ratio of shear stress at the neutral axis to the average shear stress across the cross-section. For a circular cross-section, $k'$=4/3. The shear correction factor $k'$=4/3, originally derived for homogeneous elastic beams with circular cross-sections, is adopted in this study. Although wooden dowels are anisotropic materials, the lack of available studies addressing shear correction factors for circular wooden sections necessitates the use of this conventional value. Further research is required to verify or refine this parameter by explicitly considering the influence of wood grain direction. The embedment modulus $k_{em}$ of the dowel–timber interface, expressed in N/m$^3$, is given in Table 3. The shear modulus of the dowel, $G_{d,l}$, is taken as 1400 MPa, based on data from the authors' recent study on the shear behaviour of wooden dowels [46].

To determine the stiffness $K$ within the pre-yield regime (Mode V), deformation is primarily concentrated at the interface. The general solution of (11), representing deflection behaviour, is given by (12) as proposed by Fukuyama et al. [45]. Applying fundamental principles of mechanics ((13)), the solution in (12) is further used to derive expressions for rotation $\theta_x$, bending moment $M_x$ and shear force $V_x$, considering a finite beam on an elastic foundation subjected to concentrated loading, as illustrated in Fig. 8a.

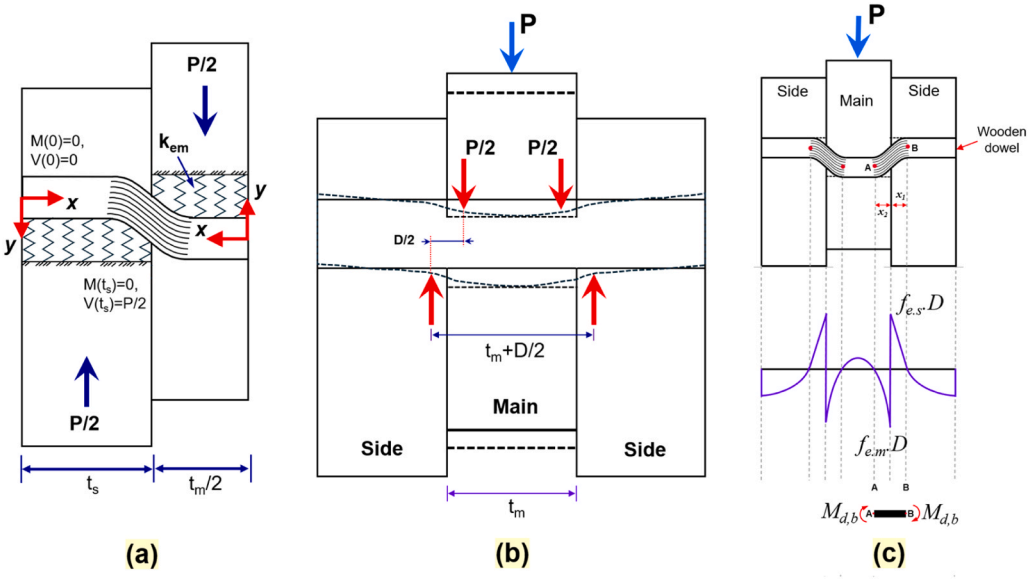


**Fig. 8.** Joint modelling approaches: (a) Beam-on-elastic-foundation (BEF) model used for joint stiffness estimation; (b) Joint stiffness model based on a simply supported beam (SSB), developed from post-test deformation observations; (c) Simplified model assuming non-uniform stress distribution.

$$\begin{cases} \lambda^4 - u_1\lambda^2 + u_2 = 0 \\ \lambda = \pm\alpha \pm \beta i \quad , \quad \alpha = \sqrt{\dfrac{\sqrt{\dfrac{k_{em}D}{EI}} + \dfrac{k'k_{em}D}{GA}}{2}}, \quad \beta = \sqrt{\dfrac{\sqrt{\dfrac{k_{em}D}{EI}} - \dfrac{k'k_{em}D}{GA}}{2}} \\ y(x) = A\cosh(\alpha x)\cos(\beta x) + B\cosh(\alpha x)\sin(\beta x) + C\sinh(\alpha x)\cos(\beta x) + D\sinh(\alpha x)\sin(\beta x) \end{cases} \tag{12}$$

$$\theta_x = \frac{dy}{dx}, \quad \frac{d^2y}{dx^2} = \frac{M_x}{EI}, V_x = \frac{dM_x}{dx}, \quad \frac{d^3y}{dx^3} = \frac{V_x}{EI} \tag{13}$$

$$\begin{bmatrix} y_x \\ \theta_x \\ \dfrac{M_x}{EI} \\ \dfrac{V_x}{EI} \end{bmatrix} = \begin{bmatrix} A & B & C & D \\ \beta B + \alpha C & -\beta A + \alpha D & \alpha A + \beta D & \alpha B - \beta C \\ u_3 A - u_4 D & u_3 B + u_4 C & -u_4 B + u_3 C & u_4 A + u_3 D \\ u_6 B + u_5 C & -u_6 A + u_5 D & u_5 A + u_6 D & u_5 B - u_6 C \end{bmatrix} \begin{bmatrix} cc_x \\ cs_x \\ sc_x \\ ss_x \end{bmatrix} \# \tag{14}$$

$$\begin{cases} u_3 = \alpha^2 - \beta^2, \quad u_4 = 2\alpha\beta, \quad u_5 = \alpha u_3 + \beta u_4, \quad u_6 = \beta u_3 - \alpha u_4 \\ cc_x = \cosh(\alpha x)\cos(\beta x), cs_x = \cosh(\alpha x)\sin(\beta x), \quad \# \\ sc_x = \sinh(\alpha x)\cos(\beta x), ss_x = \sinh(\alpha x)\sin(\beta x) \end{cases} \tag{15}$$

Constants $A$, $B$, $C$, and $D$ in (14) are integration constants arising from the reduction of (11) to the deflection solution in (12). By applying the boundary conditions defined in Fig. 8a and enforcing compatibility at the timber–dowel interface, these constants are determined. Substituting them back into (12) yields the final expression for joint stiffness, presented as (16). This formulation is applicable to single dowel connections with double shear planes and accounts for dowel bending (through the flexural modulus), dowel shear (through the shear modulus), and embedment deformation in both the dowel and timber members (through the embedment modulus).

$$K_{BEF,cal} = \sqrt{\frac{0.33(\pi E_{d,b} k_{em}^3 D^7)^{\frac{1}{2}}}{1 + \left(\frac{k_{em}E_{d,b}D}{9\pi G_{d,l}^2}\right)^{\frac{1}{2}}}} \tag{16}$$

#### 4.2.2. Joint stiffness based on post-test deformation observations

Based on the observed deformation patterns post-testing, the wooden dowel loading model illustrated in Fig. 8b is deemed appropriate. The conceptual basis of this model originates from Reference [14]. Another study also reported a similar deformed shape for weak dowels embedded in strong base timber [20]. In this model, the dowel is idealized as a simply supported beam (SSB) subjected to two-point loads ($PL$), representing the resultant forces from the central member, with the side members acting as supports. The corresponding dowel flexibility is calculated using (17), incorporating both bending and shear deformation. The shear modulus is taken as $G = E/16$, in accordance with EN 384 [47]. The bending and shear deformation components are derived using classical Euler–Bernoulli and Timoshenko beam theories. The stiffness equation ((18)) for timber members is adopted from Reference [14], where it was formulated based on a linear fit to experimental data. This equation was obtained for timber members with oven-dry specific gravity ranging from 0.40 to 0.69. This returns value in kN/mm. The overall joint stiffness is then calculated using a series spring model, as shown in (19), to determine the joint stiffness $K_{SSB,pl,cal}$.

$$K_d = \frac{1.5\pi E_{d,b} D}{\left(\frac{6t_m}{D} + 20.60\right)} \tag{17}$$

$$K_m = \frac{1}{-0.169G_t + 0.209} \tag{18}$$

$$K_{SSB,pl,\ \ cal} = \frac{K_d.K_m}{K_d + K_t} \tag{19}$$

Within the elastic range, prior to significant dowel deformation, the contact force between the dowel and central timber member may be considered as a uniformly distributed load ($UDL$). Replacing the point loads in Fig. 8b with a uniformly distributed load $P/t_m$ applied by the main member, an alternative dowel stiffness expression is derived ((20)). Using this formulation in conjunction with (18) yields the joint stiffness $K_{SSB,udl,cal}$, where $t_m$ is the thickness of the main member, $E_{d,b}$ is the dowel's elastic modulus determined from three-point bending, and $D$ is the dowel diameter.

$$K_d = \frac{\pi E_{d,b} D}{\left[7.367 + \frac{t_m}{D} + \frac{2t_m^2}{3D^2}\right]} \tag{20}$$

#### 4.2.3. Empirical models

Müller et al. proposed [48] a simplified model to estimate joint stiffness $K$per wooden dowel per shear plane, derived from linear regression fitting. This model does not account for wood species or dowel slenderness and is based on a limited dataset. This model takes $D$ in mm and returns stiffness in N/mm.

$$K_{Müller,cal} = 220D \tag{21}$$

Vilguts et al. [18] developed an equation to estimate serviceability stiffness for joints in cross-laminated timber (CLT), considering various parameters including CLT species (Douglas-Fir, Grand Fir, Western Hemlock, and Spruce-Pine-Fir), hardwood dowel species (Red Oak and Birch), and dowel diameters (19.0 mm and 25.4 mm). The model incorporates the specific gravity of the dowel ($G_d$) and the CLT ($Gc_{LT}$) and returns stiffness in kN/mm.

$$K_{Vilguts,cal} = 0.7G_d^{2.7}G_{CLT}^{0.25}D, \quad R^2 = 0.80 \tag{22}$$

#### 4.2.4. Spring in series approach

In WDTCs, the hardwood dowel is loaded perpendicular to the grain, while the timber members are loaded parallel to the grain, resulting in compression of the dowel. As stiffness is evaluated in the elastic region, where deformation is primarily governed by elastic embedment of the dowel, this behaviour can be used to estimate joint stiffness using the spring-in-series (SS) model. Alternatively, since the dowel and the timber share the same force but deform independently, their embedment stiffness can be represented as two springs in series.

$$\frac{1}{K_{SS,cal}} = \frac{1}{\alpha}\left(\frac{1}{K_t} + \frac{1}{K_d}\right) \tag{23}$$

Here, $K_d$ is the dowel stiffness (7.0688 kN/mm) obtained from isolated dowel embedment testing (*Section 2.4*), and $K_t$ is the timber stiffness, taken from the embedment stiffness of steel dowels in RP (42.33 kN/mm) and SG (63.50 kN/mm) timbers (Table 3). This approach is similar to that presented in Table 5; however, the key difference is that in Table 5 the embedment stiffness was determined experimentally, whereas in this case it is obtained through the spring-in-series approach. The factor α varies in the same manner as in Section 3.2, from 0.8 to 1. The advantage of this method is that, if the embedment stiffness values of timber ($K_t$) and dowel ($K_d$) are known, the joint stiffness can still be predicted using this formulation. This model does not require wooden dowel embedment testing in timber. The effects of dowel bending and dowel shear are incorporated through the factor α.

### 4.3. Theoretical models for yield capacity

#### 4.3.1. Regression models

Miller et al. [8] developed a least-squares regression model using experimental data and results from both physical testing and finite element simulations previously presented by Miller and Schmidt [6]. The model relates the dowel's shear stress capacity to the specific gravities of the dowel material ($G_d$) and the base timber ($G_t$). The parameter $F_{vy}$ does not represent the cross-grain shear strength of the timber fibres; rather, it corresponds to the Mode *V* yield stress within the dowel cross-section at the shear plane between the main and side members. $F_{vy}$ is defined as the yield shear stress (MPa) determined at the 5 % deformation offset. This model takes $d$ in mm and returns $P_{y,MS,cal}$ in kN.

$$P_{y,MS,\ cal,} = F_{vy}A = 0.03344G_dG_t^{0.75}.\frac{\pi D^2}{2} = 0.0525G_dG_t^{0.75}D^2 \tag{24}$$

Vilguts et al. [18] reported that (24) did not accurately predict the yield capacity of cross laminated timber connections. Their tests covered several CLT species (Douglas fir, Grand fir, Western hemlock, and spruce pine fir), hardwood dowels (red oak and birch), and dowel diameters of 19.0 mm and 25.4 mm. To address this, they proposed a modified form of (25). Notably, this revised equation does not include the specific gravity of the timber. This model takes $d$ in mm and returns $P_{y,vilguts,cal}$ in kN.

$$P_{y,vilguts,\ \ cal} = 0.031G_d^{1.1}.\frac{\pi D^2}{2} = 0.0487G_d^{1.1}.D^2 \tag{25}$$

#### 4.3.2. DIN 1052

The characteristic load-carrying capacity of a timber dowel with a constant cross-section (e.g., round) in a single or double shear WDTCs may be calculated per shear plane as follows (DIN 1052 [49]):

$$P_{y,1052,cal} = 9.5D^2 \text{ in Newton} \tag{26}$$

This equation is valid for dowel diameters 20 mm $\leq D \leq$ 30 mm, and for timber components with a characteristic density $\rho_k \geq 380$ kg/m$^3$ regardless of the angle between the force and the grain direction. The required minimum timber thickness is $t_{min}$=2$D$. For timber members with thicknesses smaller than $t_{min}$, the value of $P_{y,1052,cal}$ from (26) shall be multiplied by smaller of $t_1/t_{min}$ or $t_2/t_{min}$. $t_1$ and $t_2$ are the thicknesses of the side and main timber members, respectively.

### 4.4. Ultimate capacity calculation

#### 4.4.1. Uniform bearing stress distribution

The maximum load-bearing capacity of the connection is attained when the wooden dowel fails in bending across both the main and side members. Blass et al. [50] proposed a calculation model that aligns well with experimental results and, with modifications, can be reconciled with Johansen's theory [11]. Based on force analysis assuming uniform stress distribution, a simplified model was developed using the EYM. The simplified joint model, shown in Fig. 8c, includes a beam element A–B subjected to non-uniform stress. This model assumes a uniform stress distribution while keeping the remaining terms the same as in Fig. 8c. $M_{d,b}$ is the maximum bending moment of the dowel $M_{max}$.

Using this approach, Eq. 27 presents an analysis based on uniform stress distribution. The final expression for the ultimate load per single dowel per shear plane configuration is given by (28), denoted as $P_{u,uni,cal}$.

$$\begin{aligned} M_{d,b} + M_{d,b} - (f_e.D \times x_1)\left(x_2 + \frac{x_1}{2}\right) + (\beta f_e.D \times x_2)\left(\frac{1}{2}x_2\right) = 0 \\ F = f_eDx_1 \\ x_1 = \beta x_2 \\ x_2 = \frac{F}{f_eD\beta} \end{aligned} \tag{27}$$

$$P_{u,uni,cal} = \sqrt{\frac{M_{d,b}f_ed\beta}{1+\beta}} \tag{28}$$

$f_e$ is the embedment strength, and $\beta$=$R_e$=$f_{e,m}/f_{e,s}$ , where $f_{e,m}$ and $f_{e,s}$ are the embedment strengths of the main and side members, respectively.

#### 4.4.2. Non-uniform bearing stress distribution

To predict the ultimate shear capacity of joints, the simplified calculation model can be further refined using the fundamentals of the European Yield Model (EYM), but with a non-uniform stress distribution (Fig. 8c). Frontini et al. [5] observed that for wooden dowels with smaller diameters ($d \leq$ 20 mm), the embedment stress along the dowel surface was significantly influenced by localized deformation, leading to an uneven stress distribution. Notably, at the expected plastic hinge locations, the stress did not reduce to zero, indicating the presence of bending moments rather than purely rotational plastic behaviour. This observation suggests that the simplified assumptions of uniform stress distribution and idealized plastic hinges used in conventional embedment models do not accurately represent the actual behaviour in such cases.

Therefore, modifications should be introduced to simplified plastic hinge failure models to account for the combined effects of non-uniform bearing stress and bending, ensuring a more realistic representation of dowel behaviour under embedment loading. The bearing stresses caused by indentation largely remain within the elastic range, meaning the full bearing strength is not utilized. As a result, an uneven stress distribution develops within the fastener. The assumed non-uniform stress distribution is based on this explanation.

According to Johansen's theory [11], and with reference to Fig. 8c, a force analysis was performed. The main steps are presented in (29), which leads to (30) for calculating the ultimate shear capacity. This expression applies to the ultimate load per single dowel per shear plane configuration.

$$\begin{cases} M_{d,b}+M_{d,b}-\left(\frac{1}{2}\times f_e.d\times x_1\right)\left(x_2+\frac{x_1}{3}\right)+\left(\frac{1}{2}\times \beta f_e.d\times x_2\right)\left(\frac{2}{3}x_2\right)=0 \\ F=f_eDx_1 \\ x_1=\beta x_2 \\ x_2=\frac{F}{f_eD\beta} \end{cases} \tag{29}$$

$$P_{u,N.uni,cal}=\sqrt{\frac{3M_{d,b}f_ed\beta}{\beta+1}} \tag{30}$$

### 4.5. Discussion on the analytical models

All theoretical models presented in the preceding sections were employed to calculate the joint stiffness, yield load ($P_y$), and maximum load ($P_u$). Eurocode 5 recommends that when the mean densities ($p_{m,1}$ and $p_{m,2}$) of the two connected wood-based members differ, the density $p_m$ used in the joint stiffness equation should be taken as the geometric mean, i.e., $\rho_m = \sqrt{\rho_{m,1}\rho_{m,2}}$. For SRS-type joints, the density was determined following this method. All input parameters are taken from Section 2 (Materials and Methods). Specific gravity $G$: radiata pine (RP) = 0.490, spotted gum (SG) = 1.032, Tasmanian oak (TO) dowel= 0.599. For the TO dowel, $M_{d,b}$ = 99987.7 N·mm, diameter $D$ = 19 mm, and bending modulus $E_{d,b}$ = 8809.3 MPa. Embedment modulus $k_{em}$: TO dowel in SG = 11.05 N/mm$^3$ and in RP = 7.08 N/mm$^3$. Embedment strength $f_e$: TO dowel in SG = 14.87 MPa and in RP = 8.75 MPa. Main member thickness $t_m$: RRR and SRS = 45 mm; SSS = 42 mm. Timber embedment stiffness $K_t$: SG = 63.50 kN/mm; RP = 42.33 kN/mm. Dowel stiffness $K_d$ = 7.07kN/mm. A comparison between the experimentally obtained values and those predicted by theoretical models is provided in Table 8.

The color codes in the last three rightmost columns indicate the level of agreement between experimental and predicted values: differences within 20 % are shown in light green, differences between 20–40 % are shown in light orange, and differences greater than 40 % are shown in red.

The beam-on-elastic-foundation model ($K_{BEF,cal}$) accurately predicts joint stiffness for SSS and SRS configurations but underestimates stiffness for RRR by 24 %. It performs best among the models considered because it accounts for dowel bending through the elastic modulus, dowel shear through the shear modulus, the combined embedment of dowel and timber through the embedment stiffness, and the effect of dowel diameter. The simply supported beam models, using both point load and uniformly distributed load assumptions, provide close estimates for RRR but overestimate stiffness for SRS and SSS. This overestimation arises from the use of an empirical timber stiffness equation ((18)), which is calibrated for radiata pine and not suitable for higher-density timber such as SG. Improving the empirical equation for timber stiffness would enhance the predictive accuracy of these models. The spring-in-series approach provides accurate stiffness predictions for all cases. For SRS joints, the embedment stiffness used in the theoretical model corresponds to the lower value between RP and SG.

The applicability of the BEF, SSB, and SS models depends primarily on the availability of input parameters. The BEF model should be applied when the dowel bending and shear modulus, as well as the embedment modulus from wooden dowel embedment tests in timber, are known. The SSB model is recommended when the bending modulus is known or when the thickness of the main member varies. The stiffness $k_m$ used as input in the SSB model is obtained from (18) valid for timber members with oven-dry specific gravity ranging from 0.40 to 0.69 [14]; this limitation should be considered when applying the SSB method. The SS model is appropriate when the dowel stiffness, obtained from isolated dowel embedment tests, and the timber stiffness, taken from the embedment stiffness of steel dowels in timber, are known. This model is particularly useful for predicting the combined deformation behavior of wooden dowel–timber connections.

The empirical model by Vilguts et al. underestimates stiffness for all joints, as it was specifically developed for CLT-based systems. The overestimation for SSS, RRR, and SRS is 44 %, 62 %, and 43 %, respectively. Applying a reduction factor of 0.60 reduces the differences to within 15 %. This factor is based on the current experimental dataset and should be refined using a larger dataset. The model by Müller et al.

**Table 8**
Comparison of experimental and theoretically predicted values.

| | Calculated | | | Experimental (Table 4) | | | Calc./Exp. | | |
|---|---|---|---|---|---|---|---|---|---|
| Joint stiffness $K$ | SSS | RRR | SRS | SSS | RRR | SRS | SSS | RRR | SRS |
| $K_{Vilguts,cal}$ | 5.54 | 4.66 | 5.08 | 7.11 | 6.84 | 6.05 | 0.78 | 0.68 | 0.84 |
| $K_{SSB,pl,cal}$ | 12.90 | 5.87 | 7.52 | 7.11 | 6.84 | 6.05 | 1.81 | 0.86 | 1.24 |
| $K_{Muller,cal}$ | 8.36 | 8.36 | 8.36 | 7.11 | 6.84 | 6.05 | 1.18 | 1.22 | 1.38 |
| $K_{BEF,cal}$ | 7.14 | 5.19 | 6.24 | 7.11 | 6.84 | 6.05 | 1.00 | 0.76 | 1.03 |
| $K_{SS,cal}$ ($\alpha$=1) | 6.36 | 6.06 | 6.06 | 7.11 | 6.84 | 6.05 | 0.89 | 0.89 | 1.00 |
| $K_{SSB,udl,cal}$ | 16.95 | 6.59 | 8.83 | 7.11 | 6.84 | 6.05 | 2.38 | 0.96 | 1.46 |
| Yield capacity, $P_y$ (kN) | | | | | | | | | |
| $P_{y,Vilguts,cal}$ | 9.35 | 9.35 | 9.35 | 6.48 | 5.76 | 6.52 | 1.44 | 1.62 | 1.43 |
| $P_{y,Miller,cal}$ | 10.10 | 6.02 | 7.80 | 6.48 | 5.76 | 6.52 | 1.56 | 1.04 | 1.20 |
| $P_{y,1052,cal}$ | 6.86 | 6.86 | 6.86 | 6.48 | 5.76 | 6.52 | 1.06 | 1.19 | 1.05 |
| $P_{y,MS,cal}$ | 7.57 | 4.52 | 5.85 | 6.48 | 5.76 | 6.52 | 1.17 | 0.78 | 0.90 |
| Ultimate capacity $P_u$ (kN) | | | | | | | | | |
| $P_{u,uni,cal}$ | 7.52 | 5.77 | 5.77 | 6.80 | 5.94 | 6.96 | 1.11 | 0.97 | 0.83 |
| $P_{u,N.uni,cal}$ | 13.02 | 9.99 | 9.99 | 6.80 | 5.94 | 6.96 | 1.92 | 1.68 | 1.43 |

consistently overestimates stiffness; however, applying a 0.8 reduction factor results in predictions within 10 % of experimental values.

For yield load capacity, Vilguts et al. overestimate all cases. The formulation by Miller provides accurate predictions for RRR and SRS, but overestimates for SSS. The reason is that the Miller equation is not calibrated for high-density timber such as SG. The models by Miller and Schmidt ($P_{y,MS,cal}$) and DIN 1052 ($P_{y,1052,cal}$) offer accurate predictions with slight underestimation for RRR. TFEC 1–2019 (Timber Frame Engineering Council) [17] is the only engineering guidance that provides design provisions specific to pegged mortise and tenon timber frames. TFEC adopts the Miller formulation for predicting the capacity of wooden dowel joints. However, for dense timbers, this formulation requires refinement to achieve more accurate predictions.

For ultimate load capacity, models assuming uniform stress distribution yield accurate predictions, whereas those based on non-uniform stress distribution significantly overestimate.

Overall, considering a ± 20 % tolerance due to the inherent variability of timber, the DIN 1052 model, beam-on-elastic-foundation model, uniform stress distribution model, and spring-in-series model show excellent predictive accuracy across all joint types. The BEF model exhibited a 25 % deviation for RRR, while providing accurate predictions for the remaining cases. It is important to note that the current models have been applied only to WDTCs consisting of RP and SG, based on a limited dataset. These models were assessed against tests where only timber density (SG and RP) varied. Other variables such as dowel density, dowel diameter, side and main member thickness, and dowel slenderness ratio may also affect capacity. The applicability of the models can be strengthened by validating them across a wider range of WDTCs that include various dowel species, timber types, and joint geometries.

## 5. Conclusions

This study investigated the mechanical performance of double-shear single-dowel joints incorporating three timber combinations. Additional tests, including embedment and bending tests on TO dowels, embedment tests on TO and steel dowels in RP and SG, were conducted to better understand the behavior of WDTCs and to obtain parameters required for theoretical modelling. The key conclusions are:

- The NDS and EC5 formulations show limited applicability to WDTCs, as they significantly overestimate connection capacity. In the present study, NDS and EC5 predict the capacities of RRR, SRS, and SSS connections to be approximately 4.15, 3.51, and 5.12 times higher than the corresponding experimental values, respectively. For stiffness prediction, EC5 overestimates the experimental values by factors of 1.44 for RRR, 2.73 for SRS, and 3.90 for SSS connections. The prEN 1995–1-1 (draft EC5) model also overestimates the capacity of WDTCs; however, the magnitude of overestimation is lower than that of NDS and existing EC5. The draft EC5 predicts capacities that are approximately 1.60, 1.44, and 2.04 times higher than the experimental values for RRR, SRS, and SSS connections, respectively. The present study, together with prior work, indicates that the stiffness of WDTCs lies between 0.80 and 1.00 times the wooden dowel timber embedment stiffness $K_{em}$. Mathematically, this can be expressed as $K_{joint} = 0.80–1.00K_{em}$. This result is practically useful, as it may remove the need for additional testing to establish joint stiffness. The applicability of this relationship should be verified with larger, more diverse datasets.

- The stiffness of WDTCs is primarily governed by the elastic embedment of dowels. The COV for stiffness, yield load capacity, and ultimate load capacity were 8.28 %, 6.80 %, and 8.39 %, respectively, among the three joint types (RRR, SSS, and SRS), indicating that performance is strongly influenced by dowel behavior. Deformation characteristics differed between joint types. In the post-elastic range, dowels failed in a mixed mode comprising tensile bending and tensile shear, which is not accounted for by current EYM.
- Beam on elastic foundation, simply supported beam, and spring in series models can be used to predict joint stiffness. Beam-on-elastic-foundation models provided the most accurate predictions of joint stiffness, as they consider dowel bending, shear, and embedment contributions from both dowel and timber. Simply supported beam models better predicted RRR stiffness but require more accurate timber stiffness values for reliable SSS and SRS predictions. The spring-in-series model also gave accurate stiffness predictions and is advantageous because timber stiffness values are readily available in literature.
- For yield load capacity, the Miller and Schmidt (MS) and DIN 1052 models offered the best accuracy. A uniform stress distribution model provided better predictions of ultimate load capacity. These models can be adapted for WDTCs design by introducing safety factors and using them alongside NDS and EC5 provisions.

It is important to note that in the present study, five tests were conducted for each parameter assessment, as a small COV was observed. We recognize that the dataset is limited, and the conclusions drawn from this study are primarily based on the current set of experimental results and therefore have certain limitations. The focus of this work is on refining and developing theoretical models, with the presented tests serving to assess and validate those models. Although the proposed models demonstrated improved predictive accuracy against this limited dataset, their applicability should be further verified using wooden dowel connections across a broader range of timber densities, dowel densities, dowel diameters, and slenderness ratios. We therefore leave this as an open direction for future research and encourage independent validation and further refinement of the models. In the current study, the identification of the tension–bending + tension–shear hybrid failure of the wooden dowel is based on macroscopic failure morphology observations. Due to the confined nature of the dowel within the timber members, displacement field data from DIC and microscopic analysis of dowel cross-sections could not be obtained. Future studies should incorporate detailed displacement field measurements or microscopic investigations (e.g., crack propagation paths) to further elucidate the internal failure mechanisms of wooden dowels in WDTCs

## CRediT authorship contribution statement

**Mahmud Ashraf:** Writing – review & editing, Supervision, Conceptualization. **Mahbube Subhani:** Writing – review & editing, Supervision, Conceptualization. **Kazem Ghabraie:** Writing – review & editing, Supervision, Conceptualization. **Inayat Ullah Khan:** Writing – review & editing, Writing – original draft, Supervision, Methodology, Formal analysis, Conceptualization.

## Declaration of Competing Interest

The authors declare that they have no known competing financial interests or personal relationships that could have appeared to influence the work reported in this paper.

## Data availability

Data will be made available on request.

## References

[1] Sotayo A, Bradley D, Bather M, Sareh P, Oudjene M, El-Houjeyri I, et al. Review of state of the art of dowel laminated timber members and densified wood materials as sustainable engineered wood products for construction and building applications. Dev Built Environ 2020;1:100004. https://doi.org/10.1016/j.dibe.2019.100004.

[2] Khan IU, Subhani M, Ghabraie K, Ashraf M. Mechanical performance and design challenges of wooden fasteners: a critical analysis of evaluation methods and standards. Eur J Wood Prod 2025;83:143. https://doi.org/10.1007/s00107-025-02293-1.

[3] Interreg NWE. Towards Adhesive-Free Timber Buildings (AFTB) 2022. ⟨https://vb.nweurope.eu/projects/project-search/towards-adhesive-free-timber-buildings-aftb/⟩ (accessed March 24, 2025).

[4] StructureCraft. Dowel Laminated Timber, The All-Wood Mass Timber Panel. StructureCraft; 2024. ⟨https://structurecraft.com/materials/mass-timber/dlt-dowel-laminated-timber⟩ (accessed December 22, 2024).

[5] Frontini F, Siem J, Renmælmo R. Load-carrying capacity and stiffness of softwood wooden dowel connections. Int J Archit Herit 2020;14:376–97. https://doi.org/10.1080/15583058.2018.1547798.

[6] Miller J.F., Schmidt R.J. Capacity of pegged mortise and tenon joints. Laramie, WY 82071: University of Wyoming; 2004.

[7] Khan IU, Subhani M, Ghabraie K, Ashraf M. Exploring and refining testing approaches for hardwood dowels under axial and flexural loading: an experimental and numerical study. Wood Mater Sci Eng 2025;0:1–23. https://doi.org/10.1080/17480272.2025.2505135.

[8] Miller JF, Schmidt RJ, Bulleit WM. New yield model for wood dowel connections. J Struct Eng 2010;136:1255–61. https://doi.org/10.1061/(ASCE)ST.1943-541X.0000224.

[9] EN 1995-1-1. Eurocode 5: Design of timber structures - Part 1-1: General - Common rules and rules for buildings. Brussels, European Standard: CEN; 2008.

[10] Li H, Wei Y, Yan L, Semple KE, Dai C. Structural behavior of steel dowel-reinforced cross-laminated bamboo and timber beams. Compos Struct 2023;318:117111. https://doi.org/10.1016/j.compstruct.2023.117111.

[11] Johansen KW. Theory of timber connections. Int Assoc Bridge Struct Eng Publ 1949;9:249–62. https://doi.org/10.5169/seals-9703.

[12] Larsen H.J. The yield load of bolted and nailed joints. Proceedings of International Union of Forestry Research Organisation Division V Conference, vol. 2, Cape Town, South Africa: IUFRO-5; 1973, p. 646–55.

[13] NDS. National Design Specification (NDS) for Wood Construction. Leesburg, VA United States: American Wood Council; 2018.

[14] Sandberg LB, Bulleit WM, Reid EH. Strength and stiffness of oak pegs in traditional timber-frame joints. J Struct Eng 2000;126:717–23. https://doi.org/10.1061/(ASCE)0733-9445(2000)126:6(717).

[15] Schmidt R., MacKay R. Timber frame tension joinery. Laramie, WY 82071: Department of Civil and Architectural Engineering University of Wyoming; 1997.

[16] Schmidt R.J., Daniels C.E. Design Considerations for Mortise and Tenon. Wyoming Laramie, WY 82071: Department of Civil and Architectural Engineering University of; 1999.

[17] DeStefano J., Hershberger J., Luthi T., Lynch J., Nehil T., Schmidt D., et al. Standard for Design of Timber Frame Structures and Commentary 2019.

[18] Vilguts A, Phillips AR, Jerves R, Antonopoulos C, Griechen D. Monotonic testing of single shear-plane CLT-to-CLT joint with hardwood dowels. J Build Eng 2024;88:109252. https://doi.org/10.1016/j.jobe.2024.109252.

[19] FprEN 1995-1-1. Eurocode 5 - Design of Timber Structures - Part 1-1: General - Common Rules and Rules for Buildings 2025.

[20] Tomasi R, De Santis Y, Aloisio A, Crocetti R, Sæby VH, Nyrud AQ. Experimental and analytical investigation on timber connections with beech, birch and laminated densified wooden dowels. Constr Build Mater 2025;494:142692. https://doi.org/10.1016/j.conbuildmat.2025.142692.

[21] Pereira MC, de, Pascal Sohier M, Descamps LA, Junior T. CC. Doweled cross laminated timber: experimental and analytical study. Constr Build Mater 2021;273:121820. https://doi.org/10.1016/j.conbuildmat.2020.121820.

[22] Zhang C, Yang H, Wang Z, Wu M, Shi B, Tao H, et al. Shear characteristics of interfacial timber-to-timber joints for log-wall structures with large-diameter beech dowels: Experimental and theoretical evaluation. Constr Build Mater 2025;458:139536. https://doi.org/10.1016/j.conbuildmat.2024.139536.

[23] ABARES. Australia's forests at a glance 2019 with data to 2017–18. Canberra: ABARES); 2019.

[24] Khan IU, Subhani M, Ghabraie K, Ashraf M. Parametric study on the bending performance of wooden dowels. World Conference on Timber Engineering 2025, 2025. Brisbane, Australia: World Conference On Timber Engineering; 2025. p. 2874–80. https://doi.org/10.52202/080513-0351.

[25] Subhani M, Lui HY. Effect of primer and fibre orientation on softwood–hardwood bonding. J Compos Sci 2024;8:192. https://doi.org/10.3390/jcs8060192.

[26] Whittle L, Lock P, Hug B. Economic potential for new plantation establishment in Australia. Australian Bureau of Agricultural and Resource Economics and Sciences; 2020.

[27] Dackermann U, Elsener R, Li J, Crews K. A comparative study of using static and ultrasonic material testing methods to determine the anisotropic material properties of wood. Constr Build Mater 2016;102:963–76. https://doi.org/10.1016/j.conbuildmat.2015.07.195.

[28] Leggate W, McGavin RL, Outhwaite A, Gilbert BP, Gunalan S. Barriers to the effective adhesion of high-density hardwood timbers for glue-laminated beams in Australia. Forests 2022;13:1038. https://doi.org/10.3390/f13071038.

[29] Leggate W, McGavin RL, Outhwaite A, Dorries J, Robinson R, Kumar C, et al. The influence of mechanical surface preparation method, adhesive type, and curing temperature on the bonding of Darwin stringybark. BioResources 2021;16:302.

[30] Sotayo A, Bradley DF, Bather M, Oudjene M, El-Houjeyri I, Guan Z. Development and structural behaviour of adhesive free laminated timber beams and cross laminated panels. Constr Build Mater 2020;259:119821. https://doi.org/10.1016/j.conbuildmat.2020.119821.

[31] Sohier L. Development a new mass timber slab dowelled crosslaminated timber. Analytical design methods experimental validation. Master thesis. University Mons Universidade de São Paulo 2018.

[32] ASTM D143. Standard test methods for small clear specimens of timber. 100 Barr Harbor Drive, PO Box C700, West Conshohocken, PA, 19428-2959 USA. 2023. https://doi.org/10.1520/D0143-23.

[33] Khan IU, Subhani M, Ghabraie K, Ashraf M. Numerical simulation of wooden dowels under compression. World Conference on Timber Engineering 2025, 2025. Brisbane, Australia: World Conference On Timber Engineering; 2025. p. 2866–73. https://doi.org/10.52202/080513-0350.

[34] BS EN 408. Timber structures - Structural timber and glued laminated timber - Determination of some physical and mechanical properties. CEN, Brussels, European Standard 2010.

[35] ASTM D2395-17. Test Methods for Density and Specific Gravity (Relative Density) of Wood and Wood-Based Materials 2022. https://doi.org/10.1520/D2395-17.

[36] ASTM F1575. Standard Test Method for Determining Bending Yield Moment of Nails, Spikes, and Dowel-type Threaded Fasteners. 2024. https://doi.org/10.1520/F1575_F1575M-24.

[37] ASTM D5764. Standard Test Method for Evaluating Dowel-Bearing Strength of Wood and Wood-Based Products. 2023. https://doi.org/10.1520/D5764-97AR18.

[38] EN 383. Timber Structures — Test methods — Determination of embedment strength and foundation values for dowel type fasteners 2007.

[39] Khan IU, Subhani M, Ghabraie K, Ashraf M. Experimental and empirical study on the embedment behaviour of wooden and steel dowels in hardwood and softwood. Structures 2025;82:110708. https://doi.org/10.1016/j.istruc.2025.110708.

[40] ASTM D5652-21. Test Methods for Single-Bolt Connections in Wood and Wood-Based Products 2021. https://doi.org/10.1520/D5652-21.

[41] ISO/TR 21141. Timber structures — Timber connections and assemblies — Determination of yield and ultimate characteristics and ductility from test data. Switzerland: 2022.

[42] Fukuyama H, Ando N, Inayama M, Takemura M. Calculation model and yield process of single shear joint with wood dowel of various slendernesses. J Struct Constr Eng (Trans AIJ 2008;73:803–10. https://doi.org/10.3130/aijs.73.803.

[43] Schmidt R.J., Scholl G.F. Load Duration and Seasoning Effects on Mortise and Tenon Joints. Laramie, WY 82071: University of Wyoming; 2000.

[44] Fu H, Li Z, Alhaddad W, He M. Experimental evaluation and theoretical prediction of dowel-type joints connecting laminated veneer lumber with wood dowels. Constr Build Mater 2024;416:135248. https://doi.org/10.1016/j.conbuildmat.2024.135248.

[45] Fukuyama H, Ando N, Inayama M, Takemura M, Inoue M. Proposal of analytical models of wooden dowel shear joint (in Japanese). J Struct Constr Eng 2007;72:129–36. https://doi.org/10.3130/AIJS.72.129_4.

[46] Khan IU, Subhani M, Ghabraie K, Ashraf M. Novel approaches for shear testing of wooden dowels parallel to the grain: an experimental and numerical study. Eur J Wood Wood Prod 2026. https://doi.org/10.1007/s00107-025-02373-2.

[47] EN 384. Structural timber — Determination of characteristic values of mechanical properties and density.2004.

[48] Müller A., Vogel M., Lang S., Sauser F. Historische Holzverbindungen Untersuchung des Trag- und Lastverformungsverhaltens von historischen Holzverbindungen und Erstellung eines Leitfadens für die Baupraxis. Biel, Switzerland: Bern University of Applied Sciences (BFH) Architecture, Wood, and Civil Engineering Institute for Timber Construction, Structures, and Architecture Competence Area: Building in Existing Contexts and Monument Preservation Solothurnstrasse 102, CH-2504 Biel; 2016.

[49] DIN 1052. Entwurf, Berechnung und Bemessung von Holzbauwerken. Allgemeine Bemessungsregeln und Bemessungsregeln für den Hochbau 1999.

[50] Blass HJ, Ernst H, Werner H. Untersuchungen über die Tragfähigkeit von Verbindungen mit Holzstiften. Bau Mit Holz 1999;101:45–52.